Predictive direct flux vector control of Permanent Magnet Synchronous Motor Drives

Predictive direct flux vector control of Permanent Magnet Synchronous Motor Drives

Barbara Boazzo, Gianmario Pellegrino
Department of Energy, Politecnico di Torino, Torino, Italy

Abstract— This paper investigates a direct flux vector control strategy with minimum need of calibration, suitable for Permanent Magnet Synchronous Motor drives. The proposed controller operates in stator flux coordinates, guaranteeing the full exploitation of the inverter current and voltage limits via compact on-line computations. The reference voltage vector is obtained by means of explicit equations coming from the magnetic model of the machine, and the algorithm is insensitive to motor parameter variations, since the stator inductances are adaptively evaluated at each sample time from the observed flux components. Thus, the proposed algorithm applies to all PM machines, more or less salient or saturated, with no need of regulators tuning. Experimental tests are presented for a PM-Assisted Synchronous motor drive. Results with standard control techniques, based on proportional-integral regulators, are also reported, for the sake of comparison.

I. INTRODUCTION

Direct Torque Control (DTC) is widely adopted for AC motor drives thanks to its fast dynamics and easy implementation. It should be better named Direct Torque and Flux Control, since the controlled variables are the airgap torque and the flux amplitude. The direct control of the estimated flux magnitude facilitates the effective implementation of flux weakening in voltage limited operation [1]. The maximum current limit can be handled via torque reference saturation, with some caveat [2].

The Direct Flux Vector Control (DFVC) proposed in [3] combines the main features of Direct Torque and Flux Control schemes along with the ones of current vector controllers at constant switching frequency, taking advantage of two simple closed-loop Proportional-Integral (PI) regulators. The first one controls the flux magnitude via the direct component of the voltage vector, as many DTC schemes do, but, unlike standard DTC algorithms, the second regulator is applied to the quadrature stator current and not to the torque.

Starting from [3], the investigation has been extended towards a control strategy with minimum need of parameters tuning. A predictive version of the DFVC algorithm is presented here, where the PI-based vector control has been replaced by simple linear equations, able to relate the torque and flux references to the inverter reference voltages.

The basics of this novel control algorithm will be presented and the main challenges related to the control implementation will be highlighted as well. The mathematics behind the stator vector control will follow, together with important notes about the countermeasures needed to make the algortihm robust towards motor non linearity and cross-saturation. Then, the predictive stator current and flux observer will be introduced as key enabling technology for this closed-form control algorithm. Current and flux predictions are necessary to compensate for the delays of digital implementation. To conclude, simulation and experimental results will be provided.

The tests reported here refer to a PM-assisted Synchronous Reluctance (PMASR) motor drive, purposely chosen for its extremely non linear magnetic behavior. This machine can be considered as the most challenging example of non-linear magnetic model.

For the sake of generality, the performance of the proposed control algortihm will be compared to the ones of more common PI-Based control techniques, namely the Current Vector Control (CVC) [4] and the DFVC in [3].

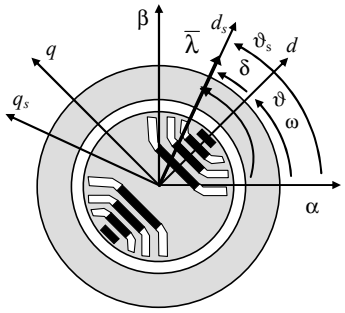

Figure 1. Reference axis frames and phase angles: stationary frame (α, β), rotor synchronous frame (d, q), stator flux synchronous frame (ds, qs); load torque angle δ, rotor position θ, stator flux synchronous frame postion θ_s.

II. BASICS OF THE PROPOSED CONTROL

The DFVC control operates in the stator flux coordinates (d_s, q_s) defined in Figure 1: the direct voltage component regulates the amplitude of the flux linkage vector λ, while the quadrature one controls the stator quadrature current i_{qs} via the load torque angle δ. Figure 1 also introduces the angle δ, the stator flux coordinate θ_s, the rotor position θ and the angular frequency ω.

A. Digital implementation of predictive controllers

The predictive control algorithm, presented here, takes advantage of the inverse machine model to relate via explicit equations the voltage command values to the torque current and flux references.

The technical challenges associated with the design of such predictive control are the nonlinear magnetic model, common to all saturated or salient PM machines, and the unavoidable delays of actuation introduced by the digital controller.

Digital, real-time controllers sample the measures from the field at the current time instant t_k and then update the voltage command one switching period (T_{sw}) later, at time t_{k+1}. The literature [5, 9] points out that the knowledge of the machine states at the actuation time t_{k+1} is necessary for obtaining a predictive control with a high dynamic performance and responses with no ringing. Thus, the control algorithm has to process the data available at the sample time t_k to predict the machine states at the execution time t_{k+1}. In other words, a predictive observer is needed. If this is

omitted, the controlled variables turn out to be oscillatory [6, 7]. Some schemes apply mitigation factors to the control error in place of the predictive observer [8], at the expense of a worst dynamics.

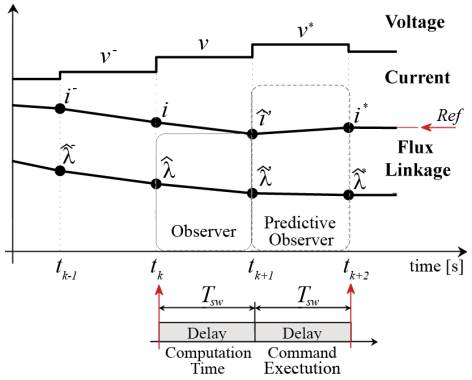

Figure 2. Sequence of the discrete time events and unavoidable delays of digital implementation. The flux linkages at t_k are estimated by a standard observer, while currents and flux linkages at t_{k+1} are given by a predictive observer (see Section IV for details).

Figure 2 provides a graphical representation of the sequence of events during consecutive sample instants and it serves as an introduction and a reminder of the notations adopted in the rest of the document.

With reference to the current sample time t_k, the superscript "–" indicates a past value (k-1), while the superscript " ' " stands for a predicted quantity (k+1). If no symbols are added, the considered variable coincides with its current value and the "hat", if present, specifies that the quantity is output by one observer and not directly measured.

Dealing with the voltage signals, the superscript "–" indicates the voltage command executed at t_{k-1} and active between t_{k-1} and t_k. The voltage vector at current time, active from t_k to t_{k+1}, is indicated with no marks. The "star" superscript indicates reference quantities: the reference voltage vector evaluated at the current period (t_k to t_{k+1}) is the voltage executed at t_{k+1} and latched until t_{k+2}. As a consequence, the flux and current references calculated at time t_k will be fulfilled not before the end of the starred voltage execution, which is at time t_{k+2}. This to put in evidence that the predictive control, at the best, can serve the current and flux set points in ***two switching periods***: one for computation plus one to complete the execution. The time to target is even longer than two execution periods if the available Volt-seconds are not sufficient to modify the machine flux linkage of the needed quantity, which is for large torque variations.

B. *Control scheme*

The blocks scheme of the proposed control algorithm is reported in Figure 3. The control sequence is described here and in the next sections.

Starting from the reference torque T^* the Maximum Torque per Ampere (MTPA) law determines the flux linkage reference λ^*. The quadrature current reference i_{qs}^* follows from the torque equation (1), given the pole pairs number p:

$$T = \frac{3}{2} p \cdot \lambda \cdot i_{qs} \tag{1}$$

The two reference quantities are limited according to the current and voltage constraints via two saturation blocks. Then the control errors are calculated by difference with the flux magnitude and q_s current component output by the predictive observer. Last, the control errors are manipulated with linear equations to obtain the reference voltage vector.

It is worth highlighting the role of the intermediate control variable $\Delta\delta$, which is the load torque angle error. This is explicitly evaluated from both the flux linkage and the quadrature current errors, and determines the quadrature voltage component as reported in Figure 3. Moreover, having the δ angle in evidence in the control chain permits to handle the Maximum Torque per Voltage (MTPV) limit very easily, via the angle error saturator reported in Figure 3 [3].

C. *Maximum current and voltage limitations*

Both the direct and the quadrature components of the current vector (i_{ds}, i_{qs}) concur to determine the amplitude of the stator current, that cannot exceed the inverter maximum limit I_{max}. The limit applied to i_{qs} is:

$$i_{qs,max} = \sqrt{I_{max}^2 - i_{ds}^2} \tag{2}$$

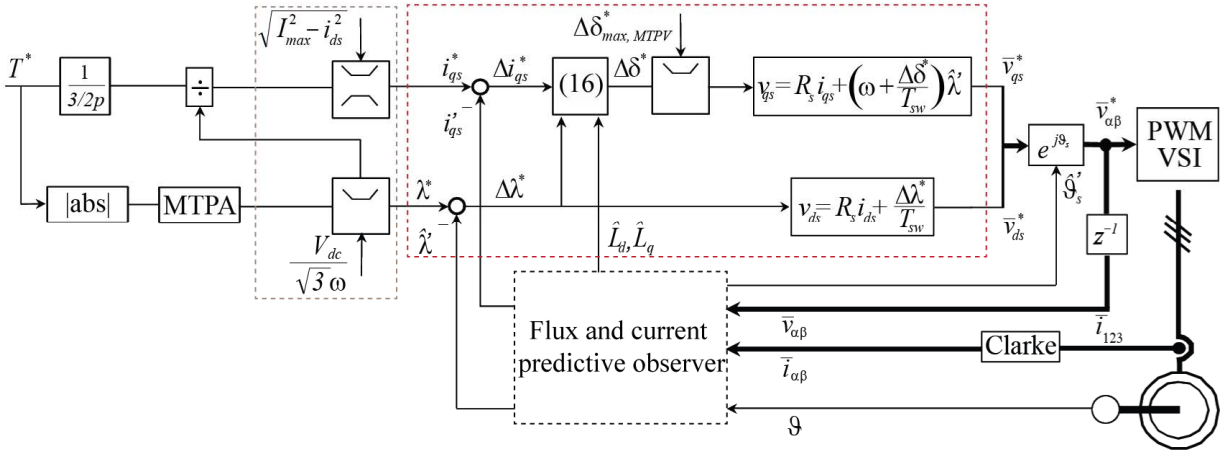

Figure 3. Predictive Direct Flux Vector Control scheme. (Dotted grey block: inverter current and voltage limitations; Dotted black block: predictive stator flux and current observer; Dotted red block: closed-form stator vector control)

The magnitude of the flux linkage vector is saturated according to the electrical operating speed ω and the maximum voltage. In formulas:

$$\lambda_{\max} = \frac{|V_{max} - R_s i_{qs}^* sign(\omega)|}{\omega} \quad (3)$$

V_{max} is a function of the dc-link voltage V_{dc} and has to be set according to the choice of exploiting or not the over modulation region. R_s is the stator resistance. Its contribution can be neglected in (3) in some cases, depending on the motor power rating.

III. CLOSED FORM STATOR VECTOR CONTROL

A. Direct and quadrature reference voltage equations

In the stator reference frame (d_s, q_s), the voltage equations are expressed as:

$$\begin{cases} v_{ds} = R_s \cdot i_{ds} + \frac{d\lambda}{dt} \\ v_{qs} = R_s \cdot i_{qs} + \left(\frac{d\delta}{dt} + \omega\right) \cdot \lambda \end{cases} \quad (4)$$

The voltage equations (4) are transposed into the discrete time domain (5), assuming a negligible variation of the electrical speed ω during the sampling period T_{sw}

$$\begin{cases} v_{ds}^* = R_s \cdot \hat{\imath}_{ds}' + \frac{\Delta\hat{\lambda}^*}{T_{sw}} \\ v_{qs}^* = R_s \cdot \hat{\imath}_{qs}' + \left(\frac{\Delta\hat{\delta}^*}{T_{sw}} + \omega\right) \cdot \hat{\lambda}' \end{cases} \quad (5)$$

Equation (5) puts in evidence that the reference voltage values are a function of time values at the actuation time t_{k+1}. In particular $\Delta\lambda^*$ and $\Delta\delta^*$ refer to t_{k+1} predictive estimations of the controlled variables (6a,b).

$$\Delta\hat{\lambda}^* = \hat{\lambda}^* - \hat{\lambda}' \quad (6a)$$

$$\Delta\hat{\delta}^* = \hat{\delta}^* - \hat{\delta}' \quad (6b)$$

The voltage model (5) relates analytically the direct voltage component v_{ds} to the desired flux variation, and the quadrature voltage component v_{qs} to the variations of the load angle δ. What it is missing now is the relationship between the load angle variation (6) to be implemented in (5) and the flux and i_{qs} errors. In the next paragraphs the load torque angle variation is expressed in terms of the control variables i_{qs} and λ by means of magnetic model manipulation.

B. Magnetic model

The magnetic model of PM machines is defined in rotor coordinates in (7). The torque expression in dq is also reported in (8) for convenience.

$$\begin{cases} \lambda_d = L_d(i_d, i_q) \cdot i_d + \lambda_m \\ \lambda_q = L_q(i_d, i_q) \cdot i_q \end{cases} \quad (7)$$

$$T = \frac{3}{2} p \left(\lambda_d i_q - \lambda_q i_d\right) \quad (8)$$

The d- and q-axis stator flux linkages (λ_d, λ_q) are defined via the PM flux linkage λ_m and the inductances L_d and L_q, which are both functions of the stator currents i_d, i_q. This occurs in general because of saturation and cross saturation effects. Figure 4a shows, as an example, the nonlinear flux linkage curves of the motor under test here (see Table I for details). The cross-coupling between the d- and q-axis is included in the self-inductance terms L_d and L_q instead of in the mutual terms L_{dq} and L_{qd} used in [10].

In the following, when addressing the stator inductances, the (i_d, i_q) bracketed term in (7) will be omitted for a shorthand notation, but the dependency of L_d, L_q on the operating condition will be always taken into. As said, those two parameters will include cross saturation.

Provided (7), a coordinates rotation to the stator field oriented reference frame (d_s, q_s) leads to (9):

$$\begin{cases} \lambda = L_{ds} \cdot i_{ds} + L_{dqs} \cdot i_{qs} + \lambda_m \cos(\delta) \\ 0 = L_{dqs} \cdot i_{ds} + L_{qs} \cdot i_{qs} - \lambda_m \sin(\delta) \end{cases} \quad (9)$$

The direct and quadrature components of the stator current vector are i_{ds} and i_{qs} respectively; the inductances defining both the d_s- and q_s-axis magnetic depend on L_d and L_q according to the flux linkage vector angle δ, as shown by (10) and (11).

$$\begin{bmatrix} L_{ds} & L_{dqs} \\ L_{dqs} & L_{qs} \end{bmatrix} = \begin{bmatrix} L_0 - \Delta L \cos(2\delta) & \Delta L \sin(2\delta) \\ \Delta L \sin(2\delta) & L_0 + \Delta L \cos(2\delta) \end{bmatrix} \quad (10)$$

$$L_0 = \frac{L_d + L_q}{2} \qquad \Delta L = \frac{L_q - L_d}{2} \quad (11)$$

Equation (12) follows from (8) and it expresses the torque in terms of the stator flux linkage magnitude and phase, instead of its d-, q-axis components.

$$T = \frac{3}{2} p \left(\frac{\lambda\lambda_m}{L_d} \sin(\delta) - \frac{\lambda^2}{2L_q} (\xi - 1) \sin(2\delta)\right) \quad (12)$$

In (12) both the magnets and the reluctance torque contributes are put in evidence, introducing the saliency ratio $\xi = L_q/L_d$.

C. Adaptive evaluation of the dq inductances

The magnetic model is the basis of the predictive control algorithm proposed here, and the inaccuracies in the parameters estimation may heavily affect the capability of deriving and performing optimal control laws [7].

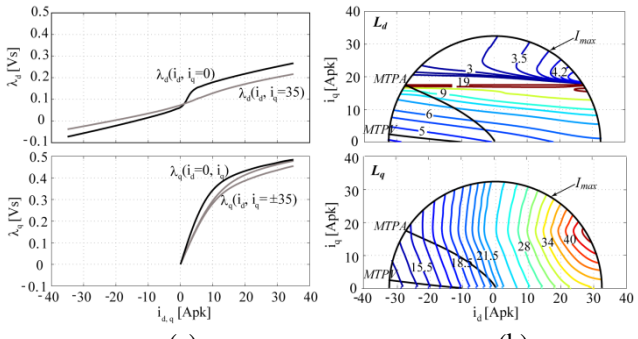

Figure 4. a) Flux linkages versus currents in the rotor reference frame; b) Level lines of inductances L_d (top) and L_q (bottom) in the d-, q-axis current plane. All plots are referred to the motor under test (see Table I for details).

For an accurate and real-time updated estimation of the machine inductances, the presented control scheme use the simple formulas (13), calculated on-line at each sample time for adaptively estimating the stator inductances from the observed flux components $\hat{\lambda}_d$ and $\hat{\lambda}_q$.

$$\begin{cases} \hat{L}_d = \frac{\hat{\lambda}_d - \lambda_m}{i_d} \\ \hat{L}_q = \frac{\hat{\lambda}_q}{i_q} \end{cases} \quad (13)$$

As said, the effects of magnetic saturation and cross saturation are included in the estimation (10), at any operating condition. Without this point to point adaptation the control would be very imprecise: Figure 4b shows that both L_d and L_q vary significantly in the *d*-, *q*-axis current plane, with reference to the example PMASR motor considered here.

D. Load angle equation

The non linear relationship (12) between the torque and the load angle δ is manipulated along with the d_s-, q_s-axis magnetic model to find the relationship between the torque current error and the corresponding δ variation.

Both the equations (9) are differentiated over a small time interval, and equations (14a,b) and (15a,b) are found, from the d_s and q_s components of (9), respectively.

$$\frac{di_{ds}}{dt} = \Lambda_{ds}\frac{d\lambda}{dt} + \mathrm{I}\Theta_{\mathrm{ds}}\frac{di_{qs}}{dt} + \Delta_{ds}\frac{d\delta}{dt} \quad (14a)$$

$$\begin{cases} \Lambda_{\mathrm{ds}} = +\frac{1}{L_0 - \Delta L\cos(2\delta)} \\ \mathrm{I}\Theta_{\mathrm{ds}} = -\frac{\Delta L\sin(2\delta)}{L_0 - \Delta L\cos(2\delta)} \\ \Delta_{ds} = -\frac{2\Delta L(\sin(2\delta)i_{ds} + \cos(2\delta)i_{qs}) - \lambda_m\sin(\delta)}{L_0 - \Delta L\cos(2\delta)} \end{cases} \quad (14b)$$

$$\frac{di_{ds}}{dt} = \mathrm{I}\Theta_{qs}\frac{di_{qs}}{dt} + \Delta_{qs}\frac{d\delta}{dt} \quad (15a)$$

$$\begin{cases} \mathrm{I}\Theta_{\mathrm{qs}} = -\frac{L_0 + \Delta L\cos(2\delta)}{\Delta L\sin(2\delta)} \\ \Delta_{qs} = -\frac{2\Delta L(\cos(2\delta)i_{ds} - \sin(2\delta)i_{qs}) - \lambda_m\cos(\delta)}{\Delta L\sin(2\delta)} \end{cases} \quad (15b)$$

The derivative of the direct current component i_{ds} is put in evidence both in (14a) and (15a), as it is the only state variable never comparing in the torque equation. The right sides of (14a) and (15a) can be equaled, so to express the derivative of the load angle δ as a function of the quadrature current and flux linkage magnitude derivatives. The resulting equation is expressed in the discrete-time domain and equation (16) is obtained.

$$\Delta\hat{\delta}^* = \frac{\Delta\hat{\imath}_{qs}^* + \frac{(\hat{\xi}-1)}{2\hat{L}_q}\cdot\Delta\hat{\lambda}^*}{\frac{\cos(\hat{\delta}')}{\hat{L}_d}\cdot\lambda_{\mathrm{m}} - \frac{(\xi-1)\cos(2\hat{\delta}')}{\hat{L}_q}\cdot\hat{\lambda}'} \quad (16)$$

$$\Delta\hat{\imath}_{qs}^* = i_{qs}^* - \hat{\imath}_{qs}' \quad (17)$$

The load angle variation (16) is a function of the control errors, the parameters of the magnetic model and the predicted magnitude and phase of the flux linkage vector.

At this point, all the linear equations needed to calculate the command voltages from the torque and flux errors are set. In fact, once i_{qs}^* and λ^* are derived, as described in Section I, and the observer outputs the predicted values of the quadrature current and the flux linkage amplitude, $\Delta\hat{\lambda}^*$ (13a) and $\Delta\hat{\imath}_{qs}^*$ (17) are determined. Equation (16) can then be applied, since $\hat{\delta}'$ is provided by the predictive observer and the estimated inductances are supposed to be approximately constant in one sample period. Eventually, the discrete-form voltage model (5) leads to the reference voltages v_{ds}^* and v_{qs}^*.

It must be noticed that the quadrature control equation (16) is coupled to direct axis quantities (the flux amplitude) only in presence of salience ($\xi \neq 1$). This confirms a well known concept that is, when dealing with salient machines, a variation of the flux amplitude always produces also a torque variation. In other words, torque regulation requires flux amplitude variations, as part of the torque is a reluctance torque, and then the inverter Volt-seconds limit becomes the main constraint to the feasible torque dynamics.

Conversely when the saliency ratio is close to one the load angle variation (16) derives from the quadrature current reference only and the d_s- and q_s-control channels are independent. It is the case of concentrated winding interior PM machines and surface PM machines, which can be both modeled by means of (4, 7) and then controlled with the proposed algorithm. In the former ones, the saliency ratio is limited by the harmonic content, while for the latter ones the parameter ξ is always close to one, and saturation effects concur to diversify the *d*- and *q*-axis magnetic behavior.

E. MTPV operation

The MTPV operation, or voltage-limited flux weakening operation, occurs at high speed when the pull-out torque limit has been reached. This condition occurs by definition when the partial derivative of the torque with respect to the load angle is equal to zero and the MTPV constraint is translated into an upper limitation (namely δ_{max}) for the load torque angle [3]. In formulas, according to (12), the MTPV condition is quantified as shown in (18).

$$\left.\frac{dT}{d\delta}\right|_{\lambda=cost} = \hat{\lambda}'\cdot\left(\frac{\cos(\hat{\delta}')}{\hat{L}_{\mathrm{d}}}\cdot\lambda_{\mathrm{m}} - \frac{(\xi-1)\cos(2\hat{\delta}')}{\hat{L}_{\mathrm{q}}}\cdot\hat{\lambda}'\right) = 0 \quad (18)$$

It is worth highlighting that the above expression determines also the validity domain of the proposed control law, since the algorithm is based on equation (16) and that expression is undetermined when its denominator is null (19).

$$\frac{\cos(\hat{\delta}')}{\hat{L}_d}\cdot\lambda_{\mathrm{m}} - \frac{(\xi-1)\cos(2\hat{\delta}')}{\hat{L}_q}\cdot\hat{\lambda}' = 0 \quad (19)$$

This result represents an important challenge, since it gives the opportunity to make the algorithm detect the MTPV operating condition autonomously and adapt the control according to, without requiring specific off-line computations.

IV. PREDICTIVE CURRENT AND FLUX OBSERVER

At each sample time t_k, the observer serves as real-time model of the physical system, to estimate the flux linkages, that cannot be measured directly, but also to predict the machine states at the instant t_{k+1}, that is when the commands are executed.

The observer operates in two consecutive steps, schematically described in Figure 5: the first one estimates the stator flux linkages at the sample time t_k, while providing the inductances estimates $\hat{L}_d$ and $\hat{L}_q$; the second one manipulates the results of the first block to predict the stator currents and flux linkages at the instant t_{k+1}. From flux and current, also the torque at t_{k+1} can be predicted.

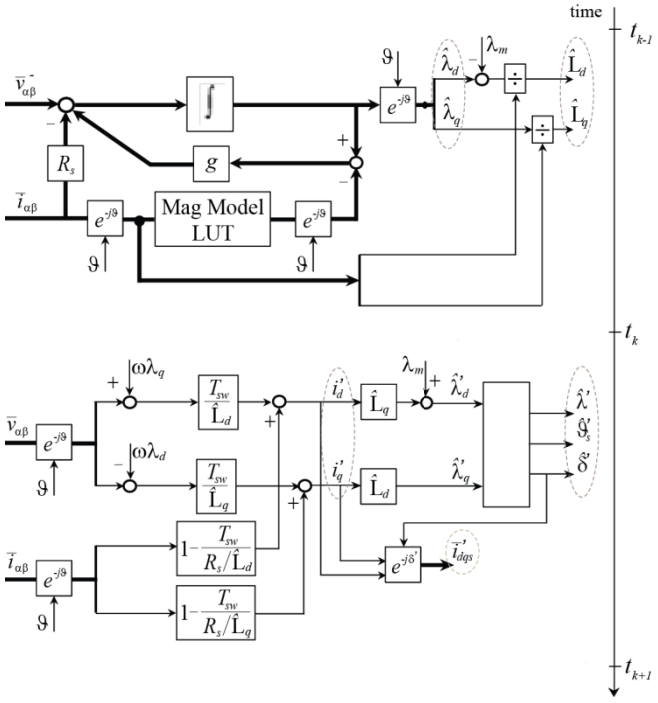

Figure 5. Predictive stator flux and current observer. The scheme is divided in two separate blocks, whose outputs are put in evidence for convenience. The first block estimates the flux linkages at the sample time t_k, while the latter one predicts the values of flux linkages and currents at the execution time t_{k+1}.

A. Observed flux at the sample time t_k

The flux linkage estimate at t_k is based on the well-known closed loop scheme where the current-to-flux model is used at low speed and the back-electromotive force integral is used at high speed [11-12].

1) Back-electromotive force integration. Figure 5 shows how to take advantage of the voltage model (20) in the stationary reference (α, β) for estimating the stator flux linkages at the sample time t_k, pointing out that the voltage command at time t_{k-1} (v^-) is used as input of the integrator.

$$\begin{cases} v_\alpha = R_s i_\alpha + \dfrac{d\lambda_\alpha}{dt} \\ v_\beta = R_s i_\beta + \dfrac{d\lambda_\beta}{dt} \end{cases} \tag{20}$$

2) Current-to-flux model. The magnetic model relates the stator currents, measured at time t_k, to the corresponding flux linkages in the (d, q) rotor frame: thus, as reported in Figure 5, coordinate rotations are needed to insert the computation in the flux observer scheme. Since this part of the observer is important only at low speed, magnetic models simples than (7) can be sometimes used, in those applications where very low speed operation is not required and/or the starting torque is moderate; otherwise, the more accurate model is preferred.

3) Crossover of the two estimation methods. The α, β flux linkages estimated by the alternative schemes 1) and 2) are combined by means of the gain g, which is expressed in radians per second and represents the crossover angular frequency between the low- and high-speed estimation methods.

4) Estimated d-, q-axis inductances. Since the proposed procedure estimates the flux linkages in the stationary frame (α, β), a coordinate rotation is needed for obtaining $\hat{\lambda}_d$ and $\hat{\lambda}_q$, and then evaluating the stator inductances applying (10).

At this point, the observer outputs are:

- the d, q stator flux linkages at the sample time t_k;
- the estimated inductances $\hat{L}_d$ and $\hat{L}_q$.

B. Predicted current and flux at the execution time t_{k+1}

Starting from the outputs of the t_k, the steps required to predict the machine states at the actuation time t_{k+1} are listed in the following:

1) Coordinate rotation of $i_{\alpha\beta}$ and $v_{\alpha\beta}$. The measured rotor position (or the estimated one in case of sensorless controllers) is used to refer to the d-, q-axis frame both the currents measured at the sample time t_k and the voltage settings, updated at the same instant.

2) Prediction of the stator d-, q-axis currents. From the voltage model in d, q coordinates (21) the stator currents (i'_d, i'_q) at the execution time t_{k+1} can be predicted.

$$\begin{cases} v_d = R_s i_d - \omega\lambda_q + \dfrac{d\lambda_\mathrm{d}}{dt} = R_s i_d - \omega\lambda_\mathrm{q} + L_d \dfrac{di_d}{dt} \\ v_q = R_s i_q + \omega\lambda_d + \dfrac{d\lambda_\mathrm{q}}{dt} = R_s i_q + \omega\lambda_\mathrm{q} + L_q \dfrac{di_q}{dt} \end{cases} \tag{21}$$

In fact, under the hypothesis that the d- and q-axis inductances are constant during one sample period, the first-order differential equations (21) can be solved and the discrete-form expressions (22) follow.

$$\begin{cases} i_d^{'} = i_d \mathrm{e}^{-\frac{R_s}{L_d}T_{sw}} + \dfrac{v_d+\omega\lambda_q}{R_s}\left(1-\mathrm{e}^{-\frac{R_s}{L_d}T_{sw}}\right) \\ i_q^{'} = i_q \mathrm{e}^{-\frac{R_s}{L_q}T_{sw}} + \dfrac{v_q-\omega\lambda_d}{R_s}\left(1-\mathrm{e}^{-\frac{R_s}{L_q}T_{sw}}\right) \end{cases} \tag{22}$$

In Figure 5 the exponentials in the two equations (22) have been are substituted with their first order Taylor approximation.

3) Prediction of the stator d-, q-axis flux linkages. Again under the assumption no inductance variations in one sample period, the predicted flux linkages λ'_d and λ'_q at the actuation time t_{k+1} are calculated from the values i'_d and i'_q by means of (7).

Also for this second stage, the outputs needed for control are highlighted in Figure 5 and listed here for convenience:

- the predicted amplitude λ' of the stator flux linkage vector at the execution time t_{k+1};
- its angular position, referred both to the stationary frame α, β (ϑ'_s) and the synchronous frame d, q (δ').
- the predicted quadrature stator current i'_{qs}.

V. VALIDATION

Experimental tests and simulations on a voltage supplied inverter PMASR motor drive have been carried out for validating the proposed control scheme and comparing its performance to the ones of more standard PI-based control techniques.

Table I summarizes the main data of the drive. The PMASR motor under test has been designed for traction and its multi-barrier rotor laminations stack is shown in Figure 6. The response of the system to the proposed control has been tested both in simulation (Matlab/Simulink), and on an experimental bench, equipped with a dSpace board and a standard incremental encoder with 512 pulses per revolution.

Figure 6. Rotor lamination of the motor under test

TABLE I. DRIVE DATA

Motor Data	
Continous power	7 kW
Peak power	10 kW
Base Speed	2200 rpm
Maximum speed	10000 rpm
Stator resistance	0.3 Ohm
Rotor inertia	4.6 10^{-3} kgm^2
Inverter Data	
Switching freq.	10 kHz
DC voltage	350 V
Maximum current	33 Apk

A. Torque step response

The torque step response and the more demanding case of torque reversal are presented first to investigate the dynamic behavior of the proposed control.

The plots reported in Figure 7 compare the experimental and simulation results for a 5 Nm torque step. Expectedly, the torque observed on the experimental rig is noisier, if compared with the one obtained in simulation, because of the sensitivity of the control to the disturbances coming from the currents measures. This undesired effect can be still mitigated, as shown in (23), by means of the attenuation coefficient k_a.

$$v_{qs}^{*} = R_s \cdot \hat{\imath}_{qs}^{'} + \left(k_a \frac{\Delta\hat{\delta}^{*}}{T_{sw}} + \omega\right) \cdot \hat{\lambda}' \qquad (23)$$

If the attenuation coefficient is close to one (e.g. 0.8), as it is the case of the results in Figure 7, it is possible to attenuate satisfactorily the noisy behavior of the torque, without compromising the dynamic response of the control.

Figure 8 the same 5 Nm torque step test repeated for three control techniques: the predictive DFVC (k_a=0.8), the PI-based DFVC of [3] and Current Vector Control with MTPA lookup tables. The different controllers lead to performances that are almost comparable: in particular the predictive algorithm guarantees the best dynamics, even if the steady state error seems to be a little greater.

B. Torque reversal

As for the torque reversal test, reported in Figure 9, analogous conclusions can be drawn in terms of dynamic response of the three control schemes. The flux vector has to move from a positive load angle to the same angle with opposite sign (or vice versa) and the available Volt-seconds represent the main limitation to the feasible dynamics, regardless the adopted control scheme.

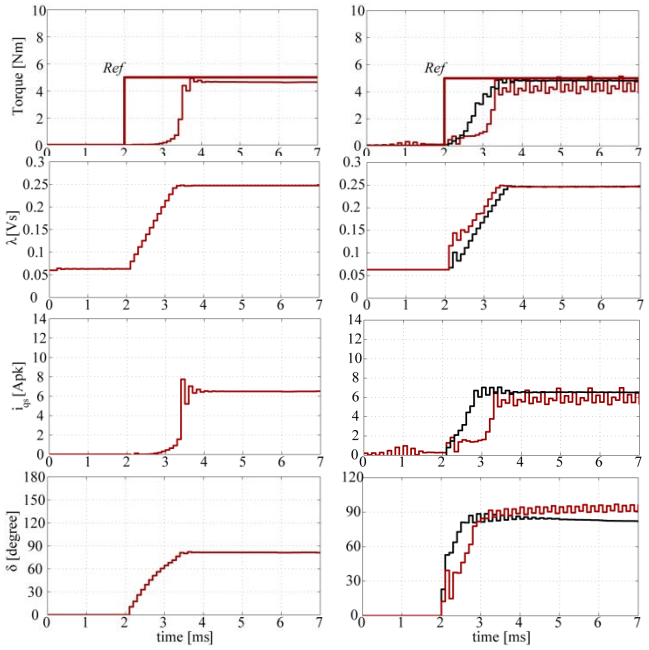

Figure 7. Simulation (left) and experimental (right) results for a 5 Nm torque step. From top to bottom: estimated torque, observed flux magnitude, quadrature current and load torque angle. As for the experimental results, the black curves refer to k_a=0.8, the red ones to k_a=1.

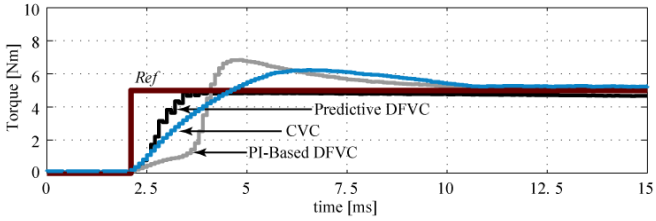

Figure 8. Experimental results for a 5 Nm torque step. For the predictive DFVC the attenutation coeffcient k_a is equal to 0.8.

Besides, torque reversal is critical for DFVC in terms of unacceptable overcurrent transients. It can happen, when dealing with salient machines and a torque reversal close to the nominal torque value: if the flux vector rotates from the motoring position to the braking position at constant amplitude it produces a transient overcurrent when encountering the PM axis, which is the minimum inductance axis. The flux magnitude must be properly weakened during the torque reversal transient. As an example, a maximum torque reversal is shown in Figure 10, where the trajectories of the current and flux linkage vectors are reported to put in evidence the consequences of improper control actions. The CVC does not have this problem, as clear from Figure 10.

It is worth noticing that the curves in Figure 9 have been obtained weakening correctly the flux magnitude during torque reversal: this demonstrates that the countermeasure proposed against undesired overcurrent transients does not compromise the achievable dynamics; in fact, as said, the performances of the two DFVC scheme are similar to the ones of the CVC, that is not affected by the same problem and that, during the reversal transient, forces both the flux linkage vector and the current one to a completely different trajectory.

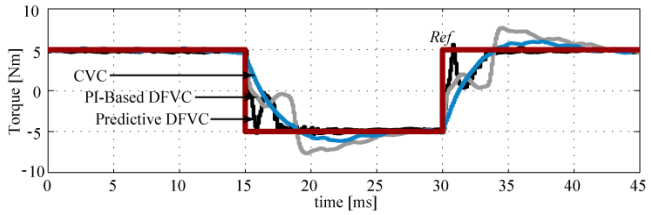

Figure 9. Experimental results for a 5 Nm torque reversal For the predictive DFVC the attenutation coeffcient k_a is equal to 0.8.

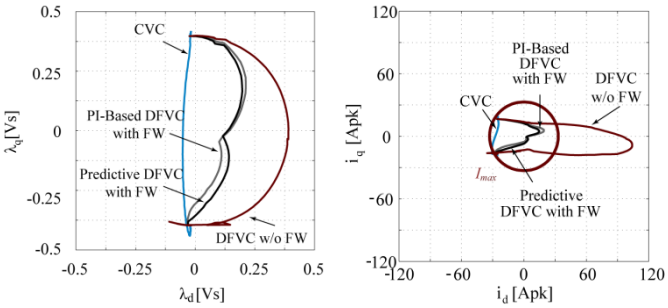

Figure 10. Simulation results: trajectories of the flux linkage and current vectors in the *d*,*q* plane during maximum torque (30 Nm) reversal. In case of direct.flux controllers, flux-weakening (FW) turns out to be a mandatory countermeasure against undesirable overcurrent transients.

C. *The predictive observer as key enabling technology*

The experimental and simulation results point out the key role played by the predictive observer. Figure 11 compares the predicted flux linkages and currents, computed by the observer, with the corresponding machine states at the execution time.

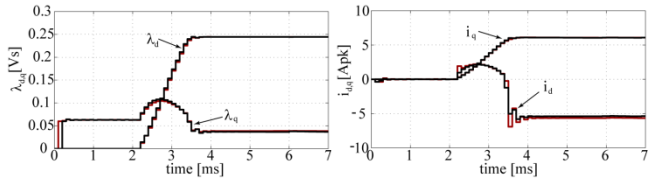

Figure 11. Simulation results for the 5 Nm torque step of Figure 7. Left: the predicted stator flux linkages (red) are compared with the actual ones (black), obtained simulating the magnetic behavior of the motor; Right: the predicted values of the stator currents (red) are compared with the measured ones (black).

Moreover, additional experimental tests have been performed purposely to put in evidence the consequences of an incorrect implementation of this enabling block. If the values of currents and flux linkages at the actuation time t_{k+1} are not predicted and if they are approximately confused with the ones at the instant t_k, the controlled quadrature current and thus the torque are affected by an intrinsic oscillatory behavior, which cannot be satisfactorily attenuated either as suggested by (23), also because large values of the attenuation factor k_a definitely compromise the feasible dynamics. This is shown in Figure 12, with reference to a 5 Nm torque step for a fair comparison with the results reported in Figure 7.

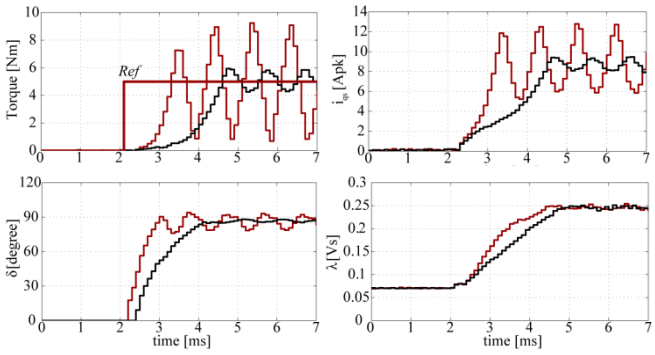

Figure 12. Experimental results: a 5 Nm torque step is applied to the controlled drive, as in the case of Figure 7, but the predictive flux observer is not implemented here. The reported signals are: the torque, the quadrature current, the observed flux magnitude and the load torque angle. The red curves refer to k_a=1, while the black ones to k_a=0.4.

D. *Effectiveness of the adaptive evaluation of L_d, L_q*

Simple tests have been carried out in simulation to validate the adaptive calculation of the stator inductances. The plots in Figure 13 summarize the results. If the *d*- and *q*-axis inductances are considered as constant values (red waveforms), referred for example to the nominal operating condition, the torque response turns out to be noisier and affected by greater steady state errors. If the inductances are evaluated as proposed, the torque response is precise at all loads.

E. *Speed step response and flux weakening*

The simulation results for speed step response are reported in Figure 14 and 15 to show the control performances in the deep flux weakening region. The reported signals are: speed and torque (Figure 14) and the DFVC controlled variables (i_{qs}, λ), along with δ (Figure 15). The MTPV operation mode and the current limitation region are put in evidence.

Again, at least in simulation, it is not possible to identify significant differences between the performances of the two DFVC schemes, namely the predictive algorithm and the PI-Based one. The speed transient in CVC is longer, accounting for a non-optimal exploitation of the torque limit profile at limited voltage and current.

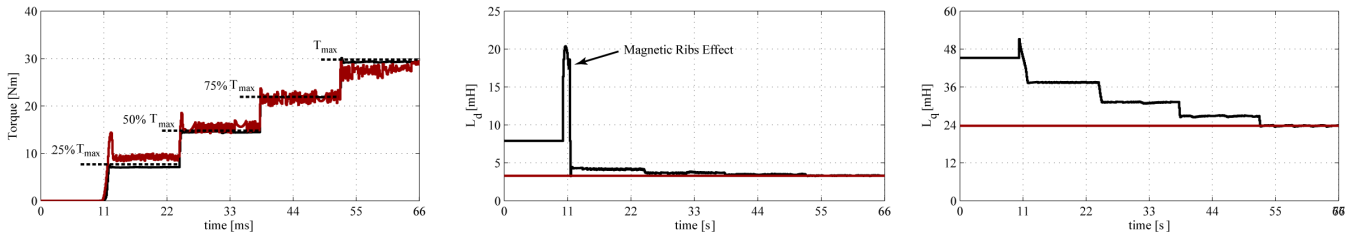

Figure 13. Simulation results: torque response with (Black) and without (Red) the adaptive calculation of the stator inductances. Plotted quantities: torque, estimated inductances. When the inductances are not adaptevely estimated, their values are assumed to be the "nominal" ones (or better they are referred to the maximum torque and the operating point is determined by the MTPA trajectory)

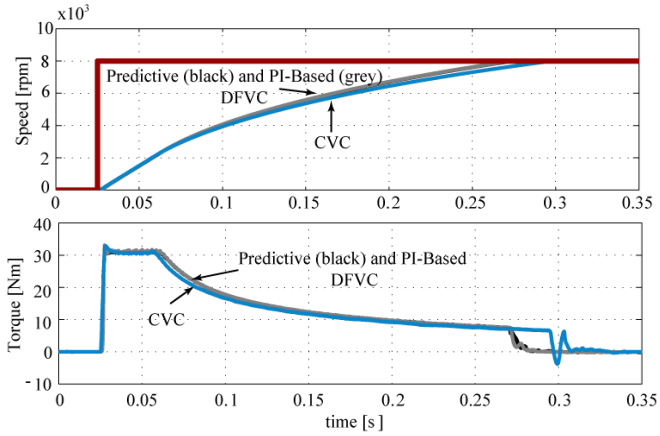

Figure 14. Simulation results: 8000 rpm speed step response.

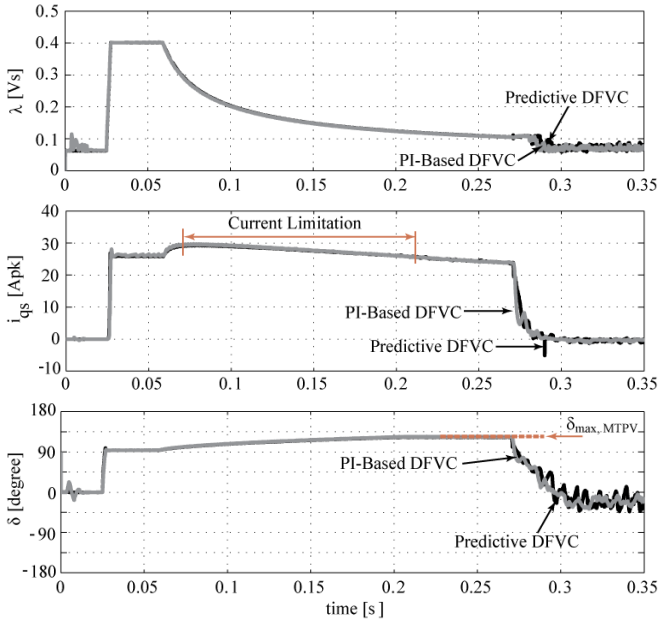

Figure 15. Simulation results: variables regulated by the Direct Flux Vector controllers during the speed transient reported in Figure 14. Top to bottom: stator flux linkage amplitude, quadrature current and load torque angle. The black curves refer to the predictive DFVC, while the grey one to the correspondent PI-Based version.

VI. CONCLUSION

The design of a predictive control algorithm based on closed form equations and insensitive to the non-linearity of the motor magnetic model has been discussed, providing experimental and simulation results to test the control performances on an IPM motor drive.

The straightforward exploitation of the inverter voltage and current limits guarantees maximum torque production under all operating conditions, including flux-weakening and MTPV operations, without requiring specific off-line computations. The adaptive evaluation of the stator inductances at each sample time improves the achievable dynamics and precision. The implementation of a predictive observer guarantees the best possible dynamic response and avoids oscillations.

The comparison with the PI-based version of the same DFVC technique says that the torque response is the best possible, while in the PI-based depends on the PI calibration and varies with the operating point. The predictive-adaptive scheme has the key advantage of not needing calibration, and it is then a valid candidate for being a universal controller for PM machines of all sizes and kinds.

REFERENCES

[1] Buja, G.S.; Kazmierkowski, M.P.; , "Direct torque control of PWM inverter-fed AC motors - a survey," Industrial Electronics, IEEE Transactions on , vol.51, no.4, pp. 744- 757, Aug. 2004

[2] Inoue, Y.; Morimoto, S.; Sanada, M.; , "Control Method Suitable for Direct-Torque-Control-Based Motor Drive System Satisfying Voltage and Current Limitations," Industry Applications, IEEE Transactions on , vol.48, no.3, pp.970-976, May-June 2012

[3] Pellegrino, G.; Bojoi, R.I.; Guglielmi, P.; , "Unified Direct-Flux Vector Control for AC Motor Drives," Industry Applications, IEEE Transactions on , vol.47, no.5, pp.2093-2102, Sept.-Oct. 2011

[4] Morimoto, S.; Sanada, M.; Takeda, Y., "Wide-speed operation of interior permanent magnet synchronous motors with high-performance current regulator," Industry Applications, IEEE Transactions on , vol.30, no.4, pp.920,926, Jul/Aug 1994

[5] Jae Suk Lee; Chan-Hee Choi; Jul-Ki Seok; Lorenz, R.D.; , "Deadbeat-Direct Torque and Flux Control of Interior Permanent Magnet Synchronous Machines With Discrete Time Stator Current and Stator Flux Linkage Observer," Industry Applications, IEEE Transactions on, vol.47, no.4, pp.1749-1758, July-Aug. 2011

[6] Kukrer, O.; , "Discrete-time current control of voltage-fed three-phase PWM inverters," Power Electronics, IEEE Transactions on , vol.11, no.2, pp.260-269, Mar 1996

[7] Maes, J.; Melkebeek, J.; , "Discrete time direct torque control of induction motors using back-EMF measurement," Industry Applications Conference, 1998. Thirty-Third IAS Annual Meeting. The 1998 IEEE , vol.1, no., pp.407-414 vol.1, 12-15 Oct. 1998

[8] Kenny, B.H.; Lorenz, R.D.; , "Stator- and rotor-flux-based deadbeat direct torque control of induction machines," Industry Applications, IEEE Transactions on , vol.39, no.4, pp. 1093- 1101, July-Aug. 2003

[9] Preindl, M.; Bolognani, S., "Model Predictive Direct Speed Control with Finite Control Set of PMSM Drive Systems," Power Electronics, IEEE Transactions on , vol.28, no.2, pp.1007,1015, Feb. 2013

[10] N. Bianchi and S. Bolognani, "Magnetic models of saturated interior permanent magnet motors based on finite element analysis," in IEEE Industry Applications Conference IAS 1998, vol. 1, Oct. 1998, pp. 27–34 vol.1.

[11] P. L. Jensen and R. D. Lorenz "A physically insightful approach to the design and accuracy assessment of flux observers for field oriented induction machine drives", IEEE Trans. Ind. Appl., vol. 30, no. 1, pp.101 -110 1994

[12] A. Vagati , M. Pastorelli , G. Franceschini and V. Drogoreanu "Digital observer-based control of synchronous reluctance motors", Conf. Rec. IEEE IAS Annu. Meeting, vol. 1, pp.629 -636 1997